

# Retina-Inspired Carbon Nitride-Based Photonic Synapses for Selective Detection of UV Light

Hea-Lim Park, Haeju Kim, Donggyu Lim, Huanyu Zhou, Young-Hoon Kim, Yeongjun Lee, Sungjin Park,\* and Tae-Woo Lee\*


Photonic synapses combine sensing and processing in a single device, so they are promising candidates to emulate visual perception of a biological retina. However, photonic synapses with wavelength selectivity, which is a key property for visual perception, have not been developed so far. Herein, organic photonic synapses that selectively detect UV rays and process various optical stimuli are presented. The photonic synapses use carbon nitride ( $C_3N_4$ ) as an UV-responsive floating-gate layer in transistor geometry.  $C_3N_4$  nanodots dominantly absorb UV light; this trait is the basis of UV selectivity in these photonic synapses. The presented devices consume only 18.06 fJ per synaptic event, which is comparable to the energy consumption of biological synapses. Furthermore, in situ modulation of exposure to UV light is demonstrated by integrating the devices with UV transmittance modulators. These smart systems can be further developed to combine detection and dose-calculation to determine how and when to decrease UV transmittance for preventive health care.

Human beings interact with their environments by perceiving and responding to external stimuli such as light, sound, pressure, and chemicals.<sup>[1–3]</sup> Among external stimuli, 80% of detected information is by the visual sense, so the retina could be considered as one of the most important part of human

Dr. H.-L. Park, H. Zhou, Dr. Y.-H. Kim, Dr. Y. Lee, Prof. T.-W. Lee  
Department of Materials Science and Engineering  
Seoul National University  
1 Gwanak-ro, Gwanak-gu, Seoul 08826, Republic of Korea  
E-mail: twlees@snu.ac.kr

H. Kim, D. Lim, Prof. S. Park  
Department of Chemistry and Chemical Engineering  
Inha University  
100 Inha-ro, Michuhol-gu, Incheon 22212, Republic of Korea  
E-mail: sungjinpark@inha.ac.kr

H. Zhou, Dr. Y.-H. Kim, Dr. Y. Lee, Prof. T.-W. Lee  
BK21 PLUS SNU Materials Division for Educating  
Creative Global Leaders  
Seoul National University  
1 Gwanak-ro, Gwanak-gu, Seoul 08826, Republic of Korea  
Prof. T.-W. Lee  
Institute of Engineering Research, Research Institute  
of Advanced Materials, Nano Systems Institute (NSI)  
Seoul National University  
1 Gwanak-ro, Gwanak-gu, Seoul 08826, Republic of Korea

 The ORCID identification number(s) for the author(s) of this article can be found under <https://doi.org/10.1002/adma.201906899>.

DOI: 10.1002/adma.201906899

bodies for perception.<sup>[4,5]</sup> A vertebrate retina possesses cone cells that detect light of a specific wavelength, and that preprocess information about their intensity, before relaying the information to the brain (Figure 1a).<sup>[6]</sup>

To emulate visual perception of retina, photonic synapses can combine two functions of sensing and synaptic elements in a single device with a more compact form than the conventional one that consists of two devices.<sup>[3,7–15]</sup> The dual functions of artificial synapse and photosensor would give abilities that are beyond those of a simple sensing device, i.e., photonic synapses can process detected light signals and track the history including light intensity, and the number, duration, and frequency of exposure.<sup>[14,16]</sup> Thus, these photonic synapses are applicable for smart sensors for the Internet of Things,

biomedical electronics, soft robots, and neural prostheses.<sup>[3]</sup>

The retinas, especially the photoreceptors, are responsible for the perception of color by detecting specific wavelength, so the combination of wavelength selectivity and signal preprocessing is a significant factor in visual perception.<sup>[3,5,17]</sup> However, development of photonic synapses that combine these abilities remains a challenge.

UV light (wavelength from 10 to 400 nm) can be harmful by causing skin aging, skin cancer, macular degeneration, and cataracts.<sup>[18–20]</sup> These problems are affected by UV intensity and by the number, duration, and frequency of exposure to UV rays.<sup>[20]</sup> The human retina cannot detect UV. Thus, by emulating the retina, photonic synapses that can selectively detect and process UV stimuli would expand the human visual sense beyond visible light and be applicable to healthcare devices.

In this study, we developed an UV-responsive photonic synapse that uses carbon nitride ( $C_3N_4$ ) layers as an UV-responsive floating-gate layer in transistor geometry. To enable modulation of the synaptic weights by UV stimulation, 2D  $C_3N_4$  nanodot materials (nanoplatelet), which were exfoliated from 3D graphitic  $C_3N_4$  particles, were used as the UV-responsive interfacial layers because they strongly absorb UV light.<sup>[21,22]</sup> The resulting photonic synapse was UV-selective. We then integrated this photonic synapse with an UV-transmittance modulator to yield a smart system to detect and block UV.

To emulate the functions of the retina,  $C_3N_4$ -based UV-responsive synaptic transistors (CNUVSs) were constructed in

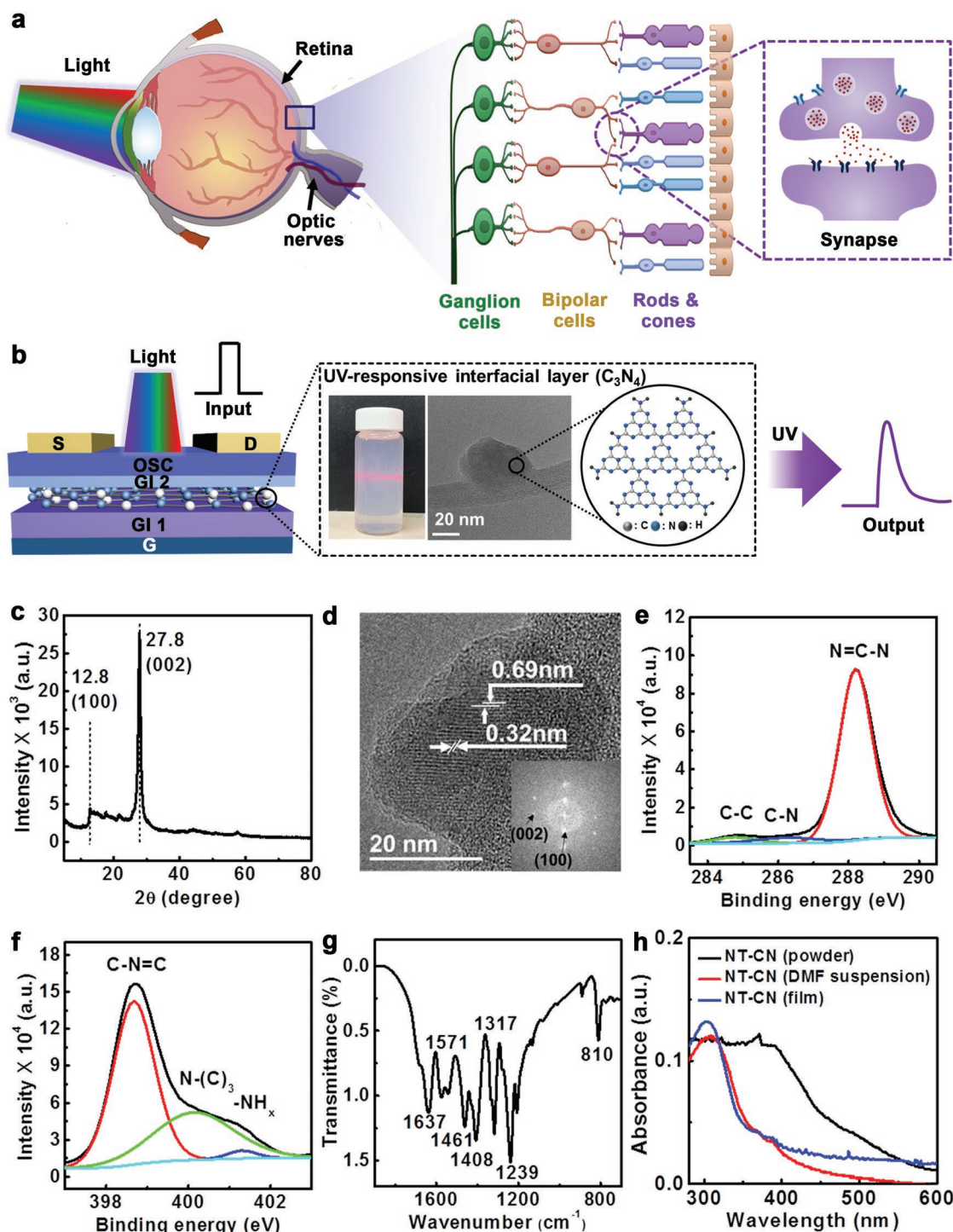


**Figure 1.** a) Schematics of a human eye in cross-sectional view and a multilayer structure of a retina. b) Schematic of device structure of the CNUVS (left panel) (S: source, D: drain, OSC: organic semiconductor, GI 1: the first gate insulator, GI 2: the second gate insulator, and G: gate) and a photograph of a homogenous colloidal DMF suspension of NT-CN with the Tyndall effect, a TEM image, and a chemical structure of NT-CN (right panel). c) An XRD pattern of NT-CN. d) A TEM image of NT-CN showing d-spacing values corresponding to the (100) and (002) lattice index (inset: FFT pattern of the TEM image). e, f) Deconvoluted XPS spectra of the NT-CN; e) C 1s and f) N 1s. g) An FT-IR spectrum of the NT-CN in a selected region (700–1900  $cm^{-1}$ ). h) UV-vis diffuse reflectance absorption spectra of NT-CN powder, suspension, and film.

the floating gate configuration in which an UV-responsive interfacial layer ( $C_3N_4$ ) was inserted between two gate insulators (Figure 1b). The  $C_3N_4$  consists of s-triazine and tri-s-triazine

units. It is inexpensive, stable against heat and chemicals, has a medium band gap, and is biocompatible and mechanically flexible,<sup>[23–26]</sup> so it is a promising material for potential use in

optoelectronics. Here, nitric acid-treated  $C_3N_4$  (NT-CN) was produced (see the Supporting Information) by the thermal treatment of melamine, then treatment of the product with  $HNO_3$ . The X-ray diffraction (XRD) pattern of the NT-CN showed peaks at  $27.8^\circ$  and  $12.8^\circ$ , which correspond, respectively, to inter-planar distances between  $C_3N_4$  layers and in-planar distances between heptazine motifs (Figure 1c).<sup>[27]</sup>

To fabricate devices using solution processes, it is highly important to produce homogenous colloidal suspensions of the NT-CN materials. Sonication of the NT-CN powder in *N,N*-dimethylformamide (DMF) produced homogenous suspensions showing the Tyndall effect (Figure 1b, inset). The suspensions showed excellent stability for at least 3 weeks (Figure S1, Supporting Information). A transmission electron microscopy (TEM) image of dried droplets of the suspension showed the presence of thin and small nanodots with a diameter of  $\approx 40$  nm (Figure 1b, inset). The 2D NT-CN nanodots were exfoliated from the 3D graphitic NT-CN powder form by the sonication.<sup>[21]</sup> TEM images detected d-spacings of 0.32 and 0.69 nm (Figure 1d), which correspond to inter-planar (002) and in-planar (100) planes, and concur with the results of a fast Fourier transformation (FFT, inset of Figure 1d) and with XRD diffraction patterns (Figure 1c).<sup>[28,29]</sup>

X-ray photoelectron spectroscopy (XPS) confirmed the formation of a  $C_3N_4$  network (Figure 1e,f). The deconvoluted XPS C 1s spectrum showed a dominant peak at 288.2 eV, which corresponds to N=C–N groups.<sup>[30,31]</sup> A peak at 284.6 eV corresponds to C–C bonds, and suggests the formation of carbon-based residue; it has often been observed previously,<sup>[28,31–34]</sup> but was very weak in the XPS measurements of the NT-CN (Figure 1e and Table S1, Supporting Information). The deconvoluted N 1s spectrum showed peaks at 398.6, 399.9, and 401.3 eV, which correspond to C–N=C, N–(C)<sub>3</sub>, and  $-NH_x$ , respectively (Figure 1f).<sup>[27,35,36]</sup> The peaks at 1637, 1571, 1461, and 1408  $cm^{-1}$  in the Fourier transform infrared (FT-IR) spectrum of the NT-CN were assignable to the heptazine rings (Figure 1g and Figure S2, Supporting Information).<sup>[28,37]</sup> Other peaks at 1317, 1239, and 810  $cm^{-1}$  correspond, respectively, to a stretching of the fully condensed C–N network, partially condensed C–NH moieties, and triazine rings.<sup>[27,28]</sup>

The absorption spectrum of DMF suspension (2D NT-CN) was considerably blue-shifted relative to that of 3D particles in a powder form (Figure 1h); this change can be attributed to the formation of 2D nanodots in the suspension from the 3D  $C_3N_4$  particle (quantum confinement effect).<sup>[21,22]</sup> The film that was formed from the suspension of 2D NT-CN showed dominantly strong absorption of UV light, as does the suspension of the 2D nanodots, but the powder of the 3D particles showed rather broad absorption from UV range to 550 nm.

A thermally grown  $SiO_2$  layer on a Si wafer was used as the first gate insulator (GI 1) (Figure 2a). The NT-CN material was deposited on the  $SiO_2$  as an UV-responsive interfacial layer ( $\approx 100$  nm of thickness). A scanning electron microscope (SEM) image of its surface showed a relatively rough surface (right panel of Figure 2a). To planarize the NT-CN layer, the second gate insulator (GI 2) of poly(methyl methacrylate) (PMMA) was formed on the NT-CN film; this process smoothed the film (right panel of Figure 2a). The PMMA also provided a tunneling layer for photo-induced charge carriers. Pentacene was

deposited as an organic semiconductor, and Au was deposited as source/drain electrodes. A cross-sectional SEM image of the device (Figure S3, Supporting Information) shows clear separation of layers. The energy-band diagram (Figure 2b) of the CNUVS in the cross-sectional direction was obtained using ultraviolet photoelectron spectroscopy and UV-vis absorption spectroscopy (Figure S4, Supporting Information).<sup>[38,39]</sup> Calculations yielded a valence band edge energy level of 5.77 eV, and a conduction band edge energy level of 2.36 eV. NT-CN had band gap energy  $E_g = 3.41$  eV, and pentacene had  $E_g = 1.77$  eV. The optical absorption spectrum of the NT-CN film covered by PMMA showed a steep rise starting from  $\approx 363$  nm, which corresponds to the  $E_g$  of NT-CN (Figure 2c). The absorbance of the NT-CN/PMMA films was strongest at 310 nm. In contrast, the pentacene film showed steep rise of optical absorption starting at  $\approx 700$  nm (which corresponds to the  $E_g$  of pentacene) and dominant peaks at 670, 585, and 280 nm (Figure 2c). The optical absorption characteristics were well-matched to the energy-band diagrams (Figure 2b,c). The absorbance of NT-CN/PMMA/pentacene film is similar to the summation of the absorbance of NT-CN/PMMA and pentacene films.

To analyze the operating principle of the CNUVS, the temporal changes in drain currents  $I_D$  were measured under red (R, 625 nm), green (G, 520 nm), blue (B, 460 nm), and UV (365 nm) light sources, each at the intensity of  $0.38$  mW  $cm^{-2}$  (Figure 2d and Figure S5, Supporting Information). We used an UV light source that had a peak wavelength of 365 nm and a spectral range from 350 to 400 nm (Figure S5, Supporting Information). At the start of illumination,  $I_D$  in the CNUVSs abruptly increased due to the photo-generation of electron–hole pairs (EHPs), irrespective of the light sources. During exposure to R, G, or B sources,  $I_D$  remained constant, but during exposure to UV light,  $I_D$  gradually increased over time. When the R, G, and B light sources were turned off, the  $I_D$  returned immediately to the initial state, but decreased gradually after the UV was turned off; this response is a slow change in channel conductivity, which is a synaptic property. Additionally,  $I_D$  was obviously higher under the B light source than under the R and G light sources (Figure 2d), even though the absorbance of the NT-CN/PMMA/pentacene film was weaker at 460 nm (the peak wavelength of B light source) than at 625 nm (R) and 520 nm (G). This difference in  $I_D$  is attributed to the absorption coefficient at each wavelength; when the pentacene film is illuminated by light with energy above  $E_g$  of the material, and the absorption coefficient is sufficiently small at that wavelength, then light with this wavelength can efficiently contribute to charge-carrier generation in the entire volume of the photo-active layer, and as a consequence increase the photocurrent that is extracted by the electrodes.<sup>[40,41]</sup>

The hypothesized mechanism of the CNUVS that shows synaptic characteristics only for UV exposure is as follows. Under UV exposure, photo-induced EHPs are generated both in the NT-CN and pentacene films (Figure 2e). The photo-induced holes in the NT-CN tunnel through the PMMA layer and are injected into the pentacene film, and the photo-induced electrons are trapped in the NT-CN films, where they form a negative potential to increase the  $I_D$  monotonically over time (Figure 2d,e). After the UV light is removed, the photo-induced EHPs in the pentacene film recombine immediately, whereas

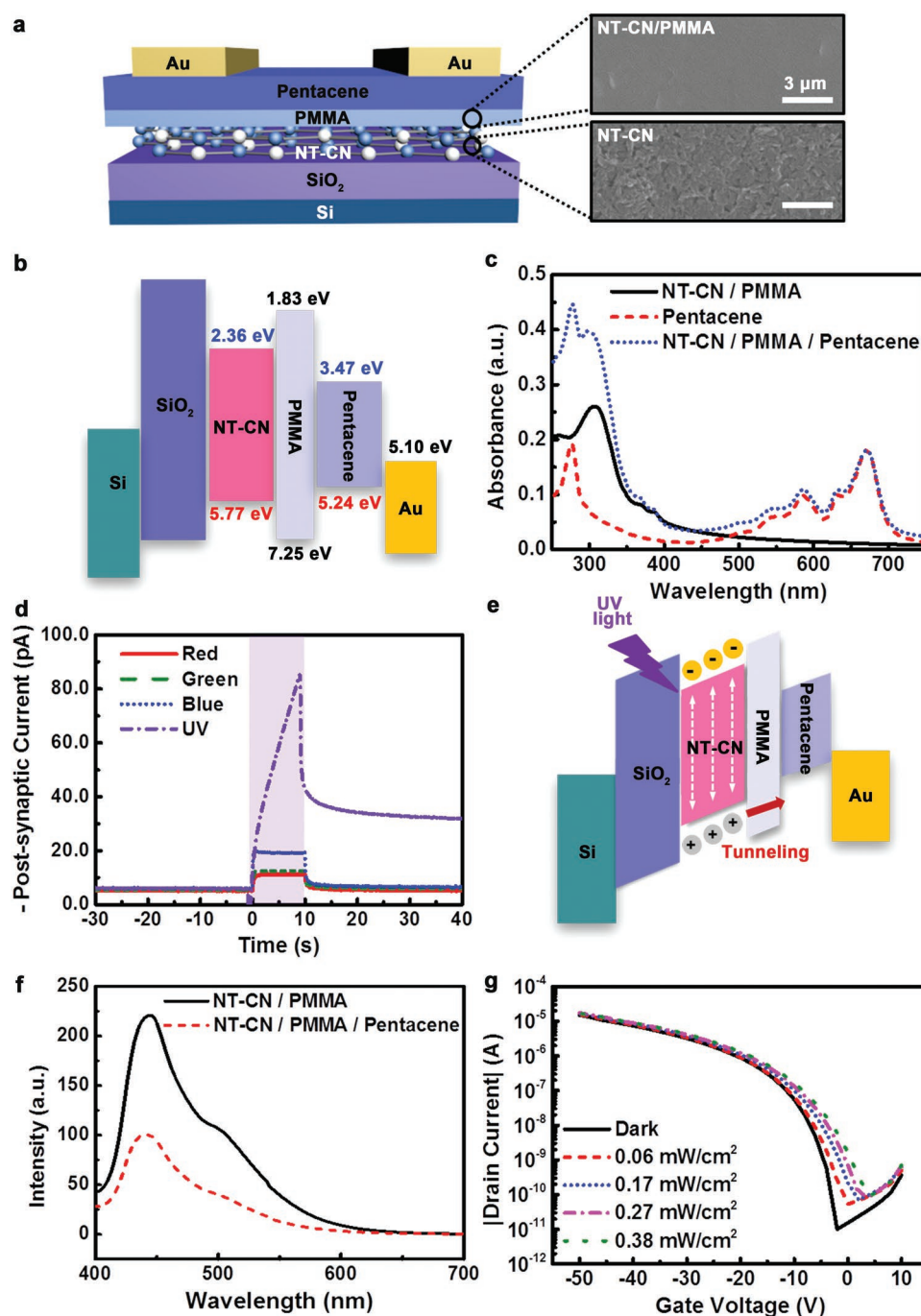


**Figure 2.** a) Schematic of the CNUVS structure with component materials (left panel) and the SEM images of NT-CN and NT-CN/PMMA films (right panel). b) Energy-band diagram of CNUVS in cross-sectional direction. c) UV-vis spectra of NT-CN/PMMA (black solid line), pentacene (red dashed line), and NT-CN/PMMA/pentacene (blue dotted line) films. d) Graphs of  $I_D$  as a function of time with R, G, B, or UV exposure ( $I_{\text{light}} = 0.38 \text{ mW cm}^{-2}$ ,  $t_{\text{light}} = 10 \text{ s}$ ) at  $V_D = -5 \text{ V}$  and  $V_G = 0 \text{ V}$ . e) Operating principle of CNUVS under UV illumination. f) Steady-state photoluminescence spectra of NT-CN/PMMA and NT-CN/PMMA/pentacene films. g) Transfer curves of CNUVSs under darkness and under illumination ( $0.06 \leq I_{\text{light}} \leq 0.38 \text{ mW cm}^{-2}$ ).

the trapped electrons in the NT-CN film cannot immediately recombine with holes and thus take long recombination time; this delay is the source of the synaptic characteristics.

To test whether photo-induced charges in the NT-CN film were injected into the pentacene layer through the PMMA layer, the photoluminescence characteristics of the

NT-CN/PMMA and NT-CN/PMMA/pentacene films were investigated (Figure 2f).<sup>[15]</sup> The peak wavelength of the excitation light source was 365 nm, which is the same as that of the UV light source. The NT-CN/PMMA/pentacene film showed lower photoluminescence intensity than the NT-CN/PMMA film; this difference means that photo-induced charges in the NT-CN

film were injected into the pentacene film through the PMMA film. The tunneling phenomena through the PMMA layer were verified by comparison with the photoresponse of the CNUVS with thicker PMMA layers (150 and 450 nm) (Figure S6, Supporting Information). The CNUVS with thicker PMMA showed no synaptic characteristics under UV illumination, but instead showed typical optical switching property.

When R, G, and B light sources were used, the  $E_g$  of NT-CN film is much higher than the photon energy of the light sources. EHPs were not photo-induced in the NT-CN film but only in the pentacene film (Figure 2b,e and Figure S5, Supporting Information). The photo-induced EHPs only in the NT-CN films contributed to the synaptic characteristics of the CNUVS by inducing the trapped electrons. R, G, or B lights did not cause synaptic characteristics in the devices, but instead just led to immediate increase of  $I_D$  under light exposure and then immediate decrease of  $I_D$  to the initial states after the light was removed; this response is an optical switching property in photodetectors. In turn, this explains the ability of the CNUVS to selectively detect UV rays for synaptic response.

To directly test the function of NT-CN films in the selective detection of UV light, a transistor without NT-CN films was fabricated (Figure S7a, Supporting Information). The device did not exhibit synaptic characteristics in response to UV exposure (Figure S7b, Supporting Information); this result is consistent with the hypothesis. Especially in organic phototransistors, PMMA layers as gate insulators do not trap charges at the PMMA/organic semiconductor interfaces, because the molecular structure of PMMA lacks charge-trapping sites such as hydroxyl groups.<sup>[42–44]</sup> Thus, in the devices that did not have NT-CN films,  $I_D$  immediately increased at the start of the light illumination due to photo-induced EHP in the pentacene layer, and remained constant during illumination because the trapping phenomenon was absent (Figure S7c, Supporting Information).<sup>[44]</sup> When the light was turned off,  $I_D$  instantly returned to its initial state; this is the same behavior in the CNUVS after exposure to R, G, and B light sources. These results prove that, among components of the CNUVSs, only NT-CN film contributes to the charge trapping and synaptic characteristics with the selective detection of UV light. The transfer characteristics (Figure 2g) of the CNUVSs demonstrate that, as the UV intensity increased,  $I_D$  increased at the same gate voltage, and the transfer curves shifted in the positive direction.

The CNUVS showed various synaptic characteristics under UV light exposure (Figure 3). Excitatory post-synaptic current (EPSC) was measured by application of UV light (peak wavelength = 365 nm, light intensity  $I_{\text{light}} = 0.38 \text{ mW cm}^{-2}$ , light pulse duration  $t_{\text{light}} = 100 \text{ ms}$ ) at drain voltage  $V_D = -10 \text{ V}$  (Figure 3a). The photonic synapses are advantageous for low energy consumption because they possess both functions of artificial synapses and photodetectors in a single device, and therefore do not require sensing elements, which use additional energy.<sup>[3]</sup> Under UV illumination with  $I_{\text{light}} = 0.38 \text{ mW cm}^{-2}$ ,  $t_{\text{light}} = 20 \text{ ms}$ , at  $V_D = -0.3 \text{ V}$ , the measured EPSC was 3.01 pA, which corresponds to an energy consumption of 18.06 fJ per synaptic event (Figure 3b). This value is comparable to the biological level (1–10 fJ per synaptic event) and, to the best of our knowledge, the lowest energy consumption yet

reported by an artificial sensory synapse (Table S2, Supporting Information).<sup>[3,45]</sup>

The CNUVS showed paired-pulse facilitation (PPF), which is a short-term potentiation (STP) property, was induced by two consecutive light pulses of  $t_{\text{light}} = 100 \text{ ms}$  separated by time interval  $\Delta t = 50 \text{ ms}$  at  $V_D = -10 \text{ V}$  (Figure 3c). The EPSC was higher after the second light pulse than after the first pulse, because the second light pulse was applied before the increased EPSC by the first one had completely decayed to the initial state. Here, a PPF index was defined as  $A_2/A_1$ , where  $A_2$  and  $A_1$  are the EPSC by the second and the first light pulses, respectively. As  $\Delta t$  decreased from 2.0 to 0.04 s, the PPF index increased from 1.04 to 1.20 (Figure 3d); this change indicates that the device has stable STP characteristics. Specifically, the PPF index was 1.030 at 1 s and 1.035 at 2 s; the difference between them is negligibly small. Thus, we conclude that PPF characteristics occurred in the CNUVS at  $\Delta t < 1 \text{ s}$ .

The CNUVS also showed spike-rate-dependent plasticity, which is one of the learning rules. To induce this change, five consecutive UV pulses were applied to the devices and EPSC gain of  $A_5/A_1$ , where  $A_5$  and  $A_1$  are EPSC levels induced by the fifth and the first light pulses, was measured at various frequencies of light-pulse trains (Figure 3e).<sup>[3]</sup> Increase in spike frequency from 1.67 to 7.14 Hz yielded an increase in  $A_5/A_1$  from 1.15 to 1.43.

The CNUVS also showed spike-duration-dependent plasticity. As  $t_{\text{light}}$  was increased from 20 to 2000 ms, the EPSC level increased from 5.14 to 82.0 pA (Figure 3f). In addition, the EPSC response of the photonic synapses was effectively controlled by the spike number and intensity of UV light (Figure 3g,h). As the spike number was increased, the post-synaptic current increased,<sup>[6,9–11,13]</sup> and a transition from STP to long-term potentiation occurred (Figure 3g). Increase in  $I_{\text{light}}$ , which governs the generation of photo-induced EHPs, increased the number of trapped electrons in the NT-CN layers, and this increase resulted in the increase in EPSCs (Figure 3h). Additionally, the CNUVS showed potentiation and depression properties (Figure S8, Supporting Information).

Finally, the smart sensing of UV by the CNUVS was examined. Changes in input (e.g., duration time and the exposure number) induced changes in the output of the CNUVSs, but not in devices that lacked NT-CN layers (Figure 4a,b). The devices without the NT-CN layer can be regarded as typical photosensors. In addition, with the increase of UV intensity, both the output of CNUVS and the control device without NT-CN increased (Figure S9, Supporting Information), i.e., both devices respond to UV intensity. However, the CNUVSs showed much higher photoresponse than the device without NT-CN (Figure S9, Supporting Information). This difference indicates that the photo-induced electrons trapped in the NT-CN layer dominantly govern the change in the channel conductivity of the devices under the UV exposure, and is consistent with the results in Figure 2 and Figure S7 in the Supporting Information.

The CNUVSs also exhibited outstanding selectivity toward UV light even under various combinations of R, G, B, and UV light sources (Figure 4c). The synaptic weight of the device was only changed by the conditions of UV exposure. These abilities of the CNUVSs to sense various types of optical information

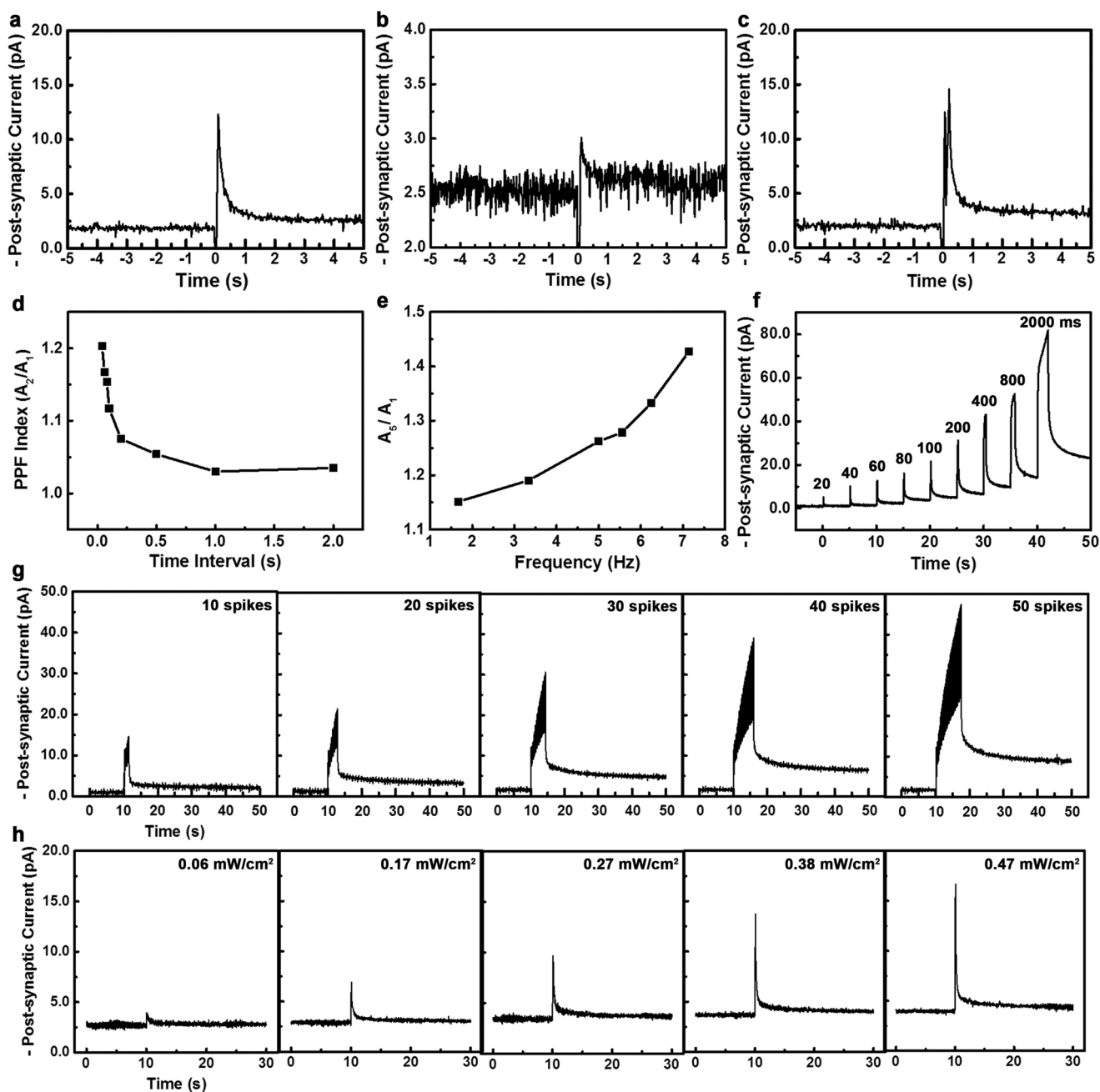


**Figure 3.** Synaptic characteristics of CNUVS under UV exposure (peak wavelength = 365 nm). a) EPSC ( $t_{\text{light}} = 100$  ms), b) minimum EPSC ( $t_{\text{light}} = 20$  ms,  $V_D = -0.3$  V), c) PPF by two consecutive light pulse ( $t_{\text{light}} = 100$  ms,  $\Delta t = 50$  ms), d) PPF index ( $A_2/A_1$ ) as a function of  $0.04 \leq \Delta t \leq 2.0$  s, e) spike-rate-dependent plasticity, f) spike-duration-dependent plasticity ( $20 \leq t_{\text{light}} \leq 2000$  ms), g) spike-number-dependent plasticity under UV light stimuli ( $I_{\text{light}} = 0.38$  mW cm $^{-2}$ ). h) EPSC under various  $I_{\text{light}}$  of UV light ( $0.06 \leq I_{\text{light}} \leq 0.47$  mW cm $^{-2}$ ).

and to selectively detect UV photons are advantageous for applications in smart sensors, artificial retina for soft humanoid robots, and neural prostheses to replace retina or interface with optic nerves.<sup>[3]</sup>

All UV exposure information including light intensity, and the number, duration, and frequency of exposure is a significant factor influencing health problems of human beings.<sup>[20]</sup> The photonic synapses described here can be used in smart systems for tracking and blocking UV light, and will have applications

in preventative health care.<sup>[20]</sup> In such systems, various types of information about UV conditions are sensed and processed to assess whether the exposure to UV ray should be modulated.

As a proof-of-concept, the CNUVS was integrated with an UV-transmittance modulator to develop a smart system to detect and block UV (Figures 4d and Figures S10 and S11, Supporting Information). For example, long UV exposure time causes health risks. This system increasingly blocked exposure to UV depending on the UV exposure duration (Figure 4e).

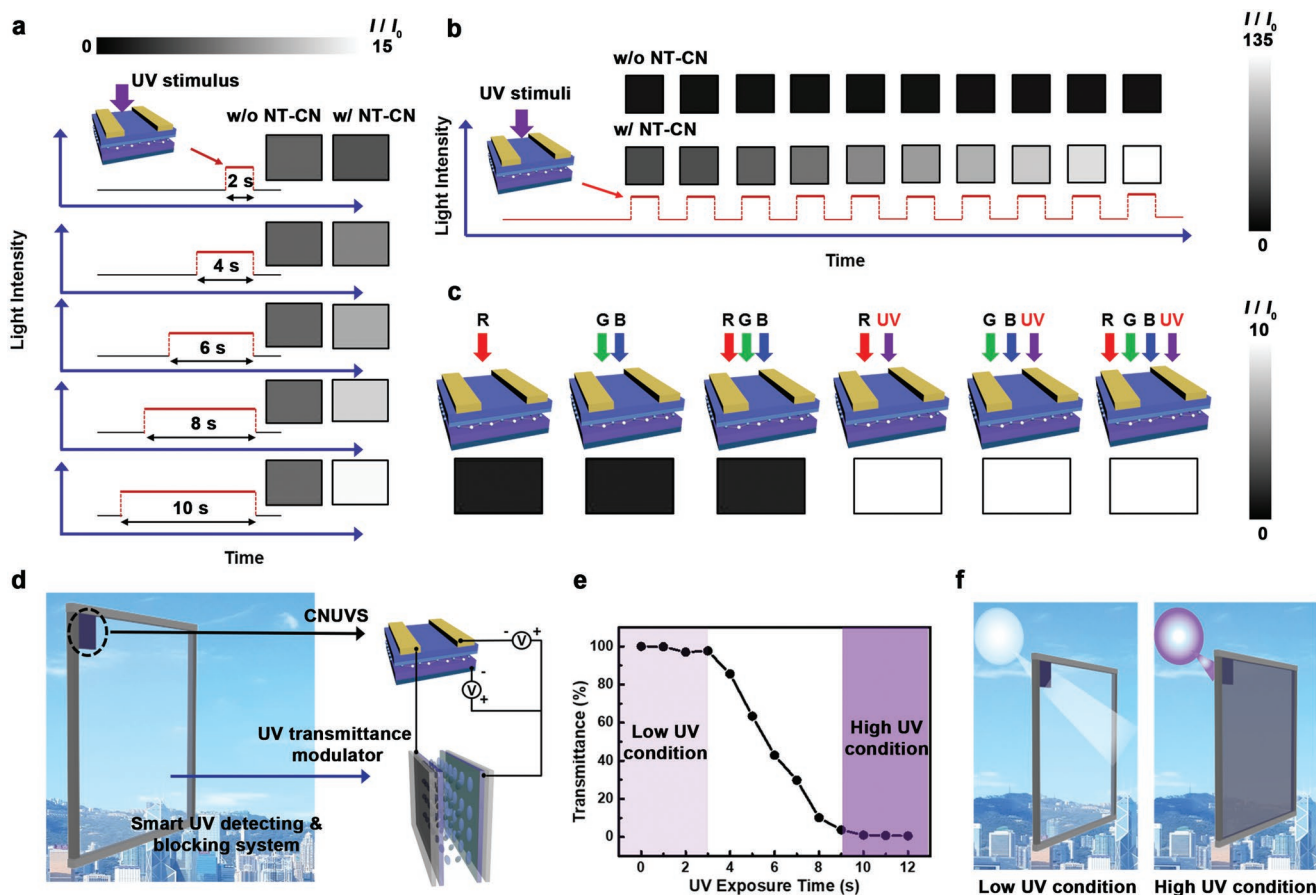


**Figure 4.** Photoresponse of devices with and without NT-CN layers under a) various durations and b) exposure numbers of UV light.  $I/I_0$  indicates the ratio of photocurrent  $I$  to the dark current  $I_0$ . c) Changes in synaptic weight of CNUVSs after exposure to various combinations of R, G, B, and UV light sources.  $I/I_0$  indicates the ratio of current  $I$  at 90 s after light off, to the initial current  $I_0$ . The synaptic weight (channel conductivity) changed only with exposure to light that included UV. d) Smart system to detect and block UV; CNUVS was integrated with the UV transmittance modulator. e) Transmittance of UV rays as a function of duration time of UV exposure on the system. f) Proof-of-concept of the smart UV detecting and blocking system.

This system can monitor in situ exposure dosage of UV rays and then control the amount of the UV exposure to reduce the health risk that it imposes (Figure 4f). Therefore, this system with the CNUVS can be regarded as an advanced system. To be applicable in reality (i.e., sunlight), the CNUVS in this system should exhibit synaptic characteristics only with UV exposure even under strong exposure that resembles sunlight. That is, the CNUVS must present synaptic characteristics under high-intensity UV exposure, whereas the devices should exhibit only typical optical switching properties even under strong intensity of other wavelengths including R, G, and B. Sunlight consists of various ranges of wavelengths including R, G, and B. Therefore, we examined the output of the CNUVS under Air Mass 1.5 Global (AM 1.5G) irradiation with a 440 nm filter to exclude UV. Under this irradiation, the devices showed only typical optical switching properties like photodetectors (Figure S12, Supporting Information), as under low-intensity R, G, and B exposure (Figure 2d).

We also measured post-synaptic current under high-intensity UV illumination similar to that in sunlight ( $\approx 4 \text{ mW cm}^{-2}$ ).<sup>[46]</sup> Under this UV irradiation, the output of the CNUVS exhibited synaptic characteristics (Figure S13, Supporting Information). As UV intensity was increased from 1 to 16  $\text{mW cm}^{-2}$ , the post-synaptic current increased (Figure S13a, Supporting Information).

Spike-number-dependent plasticity and spike-duration-dependent plasticity were also obtained under high-intensity light illumination of 4  $\text{mW cm}^{-2}$  (Figure S13b,c, Supporting Information). From these results, we conclude that the CNUVS is applicable under real sunlight.

In conclusion, we have demonstrated UV-responsive synaptic transistors that use an NT-CN layer as a UV-responsive floating-gate layer to selectively detect UV rays and to process various types of optical information by emulating the retina. We produced 2D NT-CN nanodot materials that showed a strong ability to dominantly absorb UV light, and this ability is a key factor that contributes to UV selectivity of the photonic synapses. The devices operated at an energy consumption of 18.06 fJ which is the lowest reported to date among artificial sensory synapses, and is comparable to biological level. Furthermore, to demonstrate in situ modulation of exposure to UV rays depending on the degree of UV exposure and risk, the CNUVS was integrated with the UV-transmittance modulator. This smart system to detect and block UV may be applicable to advanced electronic skin that is able to automatically adapt to the changing light-dose environment, smart windows that can selectively control transmittance of strong UV lights, smart glasses that detect and block harmful UV rays, smart sensors,

artificial retinas for soft humanoid robots, and neural prostheses compatible with biological optic nerves.

## Supporting Information

Supporting Information is available from the Wiley Online Library or from the author.

## Acknowledgements

This work was supported by the Center for Advanced Soft-Electronics funded by the Ministry of Science and ICT as Global Frontier Project (2013M3A6A5073175). This work was also supported by Creative-Pioneering Researchers Program through Seoul National University (SNU) and the National Research Foundation of Korea (NRF) grants funded by the Korea government (Ministry of Science and ICT) (NRF-2016R1A3B1908431 and NRF-2018R1A2B2003996). H.-L.P. acknowledges the support by Basic Science Research Program through the National Research Foundation of Korea (NRF) funded by the Ministry of Education (2019R1A6A3A01096063). H.Z., Y.-H.K., Y.L., and T.-W.L. acknowledge the support by the BK21PLUS SNU Materials Division for Educating Creative Global Leaders (21A20131912052).

Note: The acknowledgements section was updated on March 17, 2020, after initial publication online. In addition, the author list for affiliation 3 was corrected.

## Conflict of Interest

The authors declare no conflict of interest.

## Keywords

artificial retina, artificial synapses, photonic synapses, UV detection

Received: October 21, 2019

Revised: November 21, 2019

Published online: January 27, 2020

- [1] Y. Lee, T. W. Lee, *Acc. Chem. Res.* **2019**, *52*, 964.
- [2] Y. Kim, A. Chortos, W. Xu, Y. Liu, J. Y. Oh, D. Son, J. Kang, A. M. Foudeh, C. Zhu, Y. Lee, S. Niu, J. Liu, R. Pfattner, Z. Bao, T. W. Lee, *Science* **2018**, *360*, 998.
- [3] H. L. Park, Y. Lee, N. Kim, D. G. Seo, G. T. Go, T. W. Lee, *Adv. Mater.* **2020**, *32*, 1903558.
- [4] M. Kumar, T. Som, J. Kim, *Adv. Mater.* **2019**, *31*, 1903095.
- [5] Y. H. Jung, B. Park, J. U. Kim, T. I. Kim, *Adv. Mater.* **2019**, *31*, 1803637.
- [6] H. Wang, Q. Zhao, Z. Ni, Q. Li, H. Liu, Y. Yang, L. Wang, Y. Ran, Y. Guo, W. Hu, Y. Liu, *Adv. Mater.* **2018**, *30*, 1803961.
- [7] F. Zhou, Z. Zhou, J. Chen, T. H. Choy, J. Wang, N. Zhang, Z. Lin, S. Yu, J. Kang, H. P. Wong, Y. Chai, *Nat. Nanotechnol.* **2019**, *14*, 776.
- [8] J. Sun, S. Oh, Y. Choi, S. Seo, M. J. Oh, M. Lee, W. B. Lee, P. J. Yoo, J. H. Cho, J.-H. Park, *Adv. Funct. Mater.* **2018**, *28*, 1804397.
- [9] Y. Sun, L. Qian, D. Xie, Y. Lin, M. Sun, W. Li, L. Ding, T. Ren, T. Palacios, *Adv. Funct. Mater.* **2019**, *29*, 1902538.
- [10] M. Kumar, H. S. Kim, J. Kim, *Adv. Mater.* **2019**, *31*, 1900021.
- [11] K. Wang, S. Dai, Y. Zhao, Y. Wang, C. Liu, J. Huang, *Small* **2019**, *15*, 1900010.
- [12] Y. Zhai, X. Yang, F. Wang, Z. Li, G. Ding, Z. Qiu, Y. Wang, Y. Zhou, S. T. Han, *Adv. Mater.* **2018**, *30*, 1803563.
- [13] M. Lee, W. Lee, S. Choi, J. W. Jo, J. Kim, S. K. Park, Y. H. Kim, *Adv. Mater.* **2017**, *29*, 1700951.
- [14] X. Zhuge, J. Wang, F. Zhuge, *Phys. Status Solidi RRL* **2019**, *13*, 1900082.
- [15] Y. Wang, Z. Lv, J. Chen, Z. Wang, Y. Zhou, L. Zhou, X. Chen, S. T. Han, *Adv. Mater.* **2018**, *30*, 1802883.
- [16] Y. Zang, H. Shen, D. Huang, C. A. Di, D. Zhu, *Adv. Mater.* **2017**, *29*, 1606088.
- [17] S. Seo, S. H. Jo, S. Kim, J. Shim, S. Oh, J. H. Kim, K. Heo, J. W. Choi, C. Choi, S. Oh, D. Kuzum, H. P. Wong, J. H. Park, *Nat. Commun.* **2018**, *9*, 5106.
- [18] E. C. De Fabo, F. P. Noonan, T. Fears, G. Merlino, *Cancer Res.* **2004**, *64*, 6372.
- [19] G. P. Pfeifer, A. Besaratinia, *Photochem. Photobiol. Sci.* **2012**, *11*, 90.
- [20] R. M. Marcelo, N. Ayala, P. G. Söderberg, *Invest. Ophthalmol. Visual Sci.* **2000**, *41*, 3539.
- [21] H. Ou, L. Lin, Y. Zheng, P. Yang, Y. Fang, X. Wang, *Adv. Mater.* **2017**, *29*, 1700008.
- [22] W. F. Espinosa-García, J. M. Osorio-Guillén, C. M. Araujo, *RSC Adv.* **2017**, *7*, 44997.
- [23] W. J. Ong, L. L. Tan, Y. H. Ng, S. T. Yong, S. P. Chai, *Chem. Rev.* **2016**, *116*, 7159.
- [24] J. K. Kim, S. Park, R. J. Yoo, H. J. Jeong, J. Oh, Y. J. Lee, S. Park, D. W. Kim, *Chem. - Eur. J.* **2018**, *24*, 3506.
- [25] X. Wang, K. Maeda, A. Thomas, K. Takane, G. Xin, J. M. Carlsson, K. Domen, M. Antonietti, *Nat. Mater.* **2009**, *8*, 76.
- [26] G. Dong, Y. Zhang, Q. Pan, J. Qiu, *J. Photochem. Photobiol., C* **2014**, *20*, 33.
- [27] J. Oh, J. M. Lee, Y. Yoo, J. Kim, S.-J. Hwang, S. Park, *Appl. Catal., B* **2017**, *218*, 349.
- [28] J. Liu, T. Zhang, Z. Wang, G. Dawson, W. Chen, *J. Mater. Chem.* **2011**, *21*, 14398.
- [29] G. Zhang, G. Li, Z. A. Lan, L. Lin, A. Savateev, T. Heil, S. Zafeirotos, X. Wang, M. Antonietti, *Angew. Chem., Int. Ed.* **2017**, *56*, 13445.
- [30] N. Sun, X. Wen, Y. Tan, C. Yan, H. Wang, *Appl. Surf. Sci.* **2019**, *470*, 724.
- [31] Y. Yu, W. Yan, X. Wang, P. Li, W. Gao, H. Zou, S. Wu, K. Ding, *Adv. Mater.* **2018**, *30*, 1705060.
- [32] V. N. Khabashesku, J. L. Zimmerman, J. L. Margrave, *Chem. Mater.* **2000**, *12*, 3264.
- [33] A. P. Dementjev, A. de Graaf, M. C. M. van de Sanden, K. I. Maslakov, A. V. Naumkin, A. A. Serov, *Diamond Relat. Mater.* **2000**, *9*, 1904.
- [34] A. Vinu, K. Ariga, T. Mori, T. Nakanishi, S. Hishita, D. Golberg, Y. Bando, *Adv. Mater.* **2005**, *17*, 1648.
- [35] T. S. Miller, A. B. Jorge, T. M. Suter, A. Sella, F. Cora, P. F. McMillan, *Phys. Chem. Chem. Phys.* **2017**, *19*, 15613.
- [36] D. Dontsova, S. Pronkin, M. Wehle, Z. Chen, C. Fettkenhauer, G. Clavel, M. Antonietti, *Chem. Mater.* **2015**, *27*, 5170.
- [37] Y. Kang, Y. Yang, L. C. Yin, X. Kang, L. Wang, G. Liu, H. M. Cheng, *Adv. Mater.* **2016**, *28*, 6471.
- [38] X. Liu, G. Dong, L. Duan, L. Wang, Y. Qiu, *J. Mater. Chem.* **2012**, *22*, 11836.
- [39] S. Cui, Y. Hu, Z. Lou, R. Yi, Y. Hou, F. Teng, *Org. Electron.* **2015**, *22*, 51.
- [40] Y. Hu, G. Dong, L. Wang, Y. Qiu, *Jpn. J. Appl. Phys.* **2006**, *45*, L96.
- [41] A. El Amrani, B. Lucas, F. Hijazi, A. Moliton, *Mater. Sci. Eng., B* **2008**, *147*, 303.
- [42] H.-L. Park, S.-H. Lee, M.-H. Kim, H. Kim, *Semicond. Sci. Technol.* **2019**, *34*, 075006.
- [43] B. Mukherjee, M. Mukherjee, Y. Choi, S. Pyo, *ACS Appl. Mater. Interfaces* **2010**, *2*, 1614.
- [44] H.-L. Park, I.-H. Lee, C.-M. Keum, S.-H. Lee, S.-D. Lee, *Thin Solid Films* **2016**, *619*, 297.
- [45] W. Xu, S. Y. Min, H. Hwang, T. W. Lee, *Sci. Adv.* **2016**, *2*, e1501326.
- [46] R. Haywood, *Photochem. Photobiol.* **2006**, *82*, 1123.